Macromolecular Chemistry and Physics
www.mcp-journal.de

Analysis of the Local Mobility of RAFT Mediated Poly(acrylic acid) Networks via Low Field ^{1}H-NMR Techniques for Investigation of the Network Topology

Federica Cavalli, Christoph Pfeifer, Lukas Arens, Leonie Barner, and Manfred Wilhelm**

An in-depth investigation of the network topology for a series of sodium acrylate hydrogels synthesized via conventional free radical polymerization (FRP) and reversible addition–fragmentation chain transfer (RAFT) polymerization is conducted. The role of the RAFT agent on the crosslinking process is demonstrated on a model system upon analysis of the reaction mixture via size-exclusion chromatography before the gelation point. For a comprehensive study, both the impact of the amount of RAFT agent and of the degree of crosslinking on the microstructure of the final product are systematically investigated. In addition to swelling experiments and oscillatory shear rheology measurements, the resulting networks are analyzed via low-field proton nuclear magnetic resonance (^{1}H-NMR) techniques such as transverse relaxation and double-quantum coherence to evaluate the network mobility, which is then correlated to structural inhomogeneity. A broader mobility distribution is observed for the RAFT mediated networks compared to the FRP samples, which can be assigned to a higher content of dangling ends in the former case. The results are further elaborated to propose a mechanism for network formation in presence of a RAFT agent.

1. Introduction

Polymer networks are a 3D assembly of polymer chains physically or covalently crosslinked with each other.[1–3] The particular microstructure of polymer networks makes the material insoluble, so that in contact with solvent it swells rather than dissolve.[4] The swelling ability mainly depends on the affinity of the gel for the solvent, which in turn is determined by the chemistry of the polymer backbone.[5] For example, hydrogels are networks able to swell in water due to the presence of hydrophilic groups on the polymer chain.[6] The water absorbency is substantially enhanced if permanent charges are introduced within the network microstructure.[7,8] In the aforementioned case, the materials are referred to as polyelectrolyte gels or superabsorbent polymers (SAPs). The improved absorbency makes SAPs a relevant material on the industrial scale.[9] The production of SAPs reached 3.2 Mt per year in 2015,[10] with poly(sodium acrylate) (PSA) covering 65% of the market share.[11] The main usage of SAPs finds space in personal hygiene products,[12] soil conditioners in agriculture,[13] and specifically designed coatings for underwater-cable sealing.[14] Furthermore, new promising applications such as separation agent for the desalination of salt water[15–17] or to recover energy in an osmotic engine[18] was recently proposed. Aside the chemical composition, also the network microstructure plays an important role for the achievement of, for instance, ultra-tough hydrogels[19] and more homogeneous network topologies to improve mechanical strength and swelling ability.[20] It was shown that structural defects, such as primary and secondary loops, negatively affect the elasticity of the network,[21,22] while dangling ends and unreacted moieties influence the pore size distribution and thus the swelling ability.[23] Although the presence of defects is currently still inevitable during the crosslinking process,[24] current research focuses on the development of new synthetic methods to limit their formation.[25–27] At the same time, the expansion of analytical tools to detect the presence of defects and to investigate their impact on the final properties of the gel plays a key role.[22,28,29]

On a large scale, polymer networks are often synthesized via conventional free radical polymerization (FRP),[30] which allows only a poor control over the network microstructure leading to hydrogels with an undefined pore size distribution and crosslinking density.[1] To overcome this problem, starting from the pioneering work of Ide and Fukuda,[31,32] the use of controlling agents is proposed in the literature as a simple tool for the achievement of more homogeneous network microstructures.[33–35] This idea is based on the controlled growth

Dr. F. Cavalli, Prof. L. Barner
Soft Matter Synthesis Laboratories
Institute for Biological Interfaces
Karlsruhe Institute of Technology
Hermann-von-Helmholtz Platz 1, 76344 Eggenstein-Leopoldshafen, Germany
E-mail: leonie.barner@qut.edu.au
C. Pfeifer, Dr. L. Arens, Prof. M. Wilhelm
Institute for Chemical Technology and Polymer Chemistry
Karlsruhe Institute of Technology
Engesserstrasse 18, 76131 Karlsruhe, Germany
E-mail: manfred.wilhelm@kit.edu
Prof. L. Barner
Institute for Future Environments
Queensland University of Technology
2 George St, Brisbane, Queensland 4000, Australia

DOI: 10.1002/macp.201900387

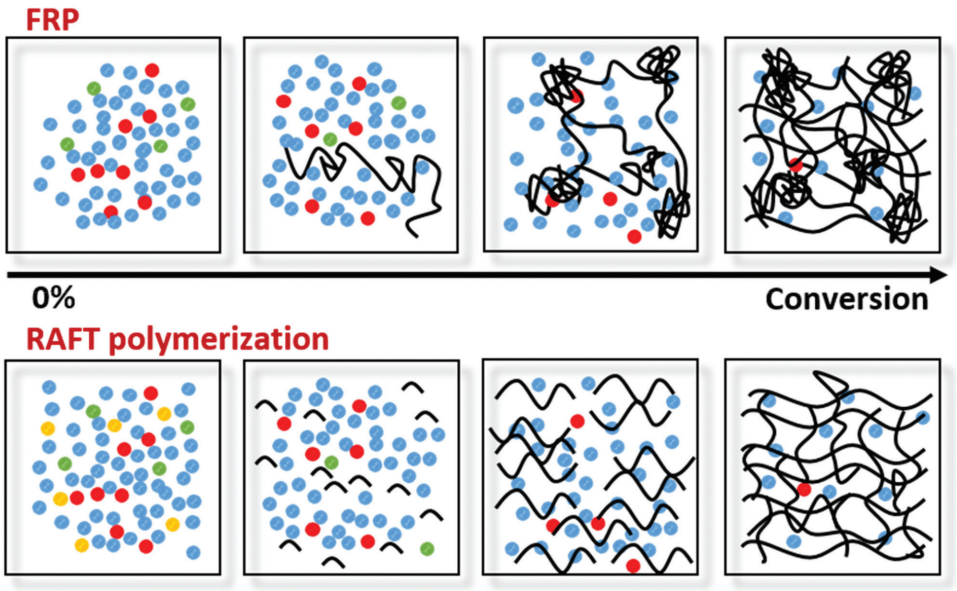

Figure 1. Comparison of the crosslinking process for the conventional free radical polymerization (FRP) and the reversible addition–fragmentation chain transfer (RAFT) polymerization of the monomer (blue), initiator (green), crosslinker (red), and RAFT agent (yellow) as proposed in the literature.[33] The main difference between the two processes is the length of the polymer chain at low conversion. Particularly, the FRP is characterized by long chains at early stage, which can lead to the formation of nanogel, and thus networks with both high and low crosslinked domains. The RAFT polymerization in contrast, allows for a higher control of the molecular weight of the growing chains, a better diffusion of the growing radicals, and potentially to a more homogeneous network microstructure.[33]

of the radicals during the crosslinking process, as shown in **Figure 1**, and gained increasing interest due to the possibility to adapt the concept to different vinyl/divinyl monomer combinations upon a proper selection of the controlling agent. Another advantage is the facile experimental set-up, and the possibility to achieve polymer networks in one-pot synthesis, similar to FRP. Nevertheless, recent reports disputed the homogeneity of networks obtained via "living" polymerizations.[36–38]

Concerning the characterization of polymer networks, the challenges are associated with the insolubility of the analyte as well as the complexity of its microstructure.[20,39] The commonly performed swelling experiments[8] and oscillatory shear rheology measurements[40] generally describe differences in the crosslinking density with only one mean value. However, for a complete picture, the network microstructure needs to be resolved at different length scales.[20] In the range between 10 and 100 nm information on the network topology are obtained via scattering techniques,[41] such as dynamic light scattering (DLS),[42] or small angle neutron scattering (SANS).[43] The length scales below 10 nm refer to the size of the single mesh.[20] Analytical techniques working in this range allow for the detection of loops, unreacted moieties, and dangling ends. In this context, few groups reported the possibility to quantify the presence of unreacted moieties,[44–46] while Johnson and coworkers developed a procedure for the quantification of primary and secondary loops.[28,47] In addition, the pore size distribution can be determined by evaluating the diffusion of probing species of known size within the network matrix.[48] Some examples include the diffusion of either non-charged polymers evaluated via inverse size exclusion chromatography,[49] or of magnetic particles upon application of magnetic fields.[50]

Recently, the analysis of the network structure via low-field ^{1}H-NMR techniques, such as T_2 relaxation and double quantum ^{1}H-NMR (DQ-NMR), was discussed in the literature as a powerful tool for correlating differences in mobility to structural inhomogeneity.[51,52] The concept is based on the fact that the network is composed of structural elements with significant different mobility, for example, crosslinking points are rigid, dangling ends and loops are mobile, while the mobility of the elastic chains increases with increasing the length of the chains itself.

In the current study, the synthesis of superabsorbent polymers based on poly(sodium acrylate) (PSA) is performed via reversible addition–fragmentation chain transfer reaction (RAFT) particularly focusing on the impact of the controlling agent on both the crosslinking process, and on the final network structure. With the aim of gaining insight into the network topology, and on how different synthetic parameters affect the final material, a series of networks with a fixed degree of crosslinking (DC) and different amounts of RAFT agent, varying from 0 to 1 mol% were synthesized first. Subsequently, the RAFT content was fixed at 0, 0.10, and 0.25 mol% and the DC varied between 0.6 and 5 mol%. All networks were characterized by swelling tests, oscillatory shear rheology, and low-field ^{1}H-NMR techniques such as T_2 relaxation and DQ experiments.

2. Experimental Section

2.1. Materials

Prior to use acrylic acid (AA, 99%, Sigma-Aldrich) was distilled, azobis(isobutylnitril) (AIBN, 98%, Merck) was recrystallized,

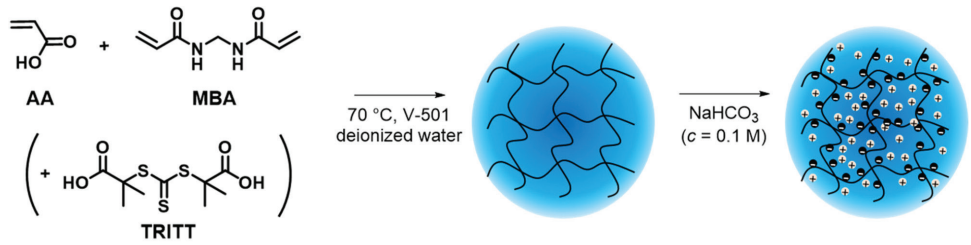

Figure 2. Reaction scheme for the achievement of poly(sodium acrylate) hydrogels. First the poly(acrylic acid) network is synthesized, with or without the presence of TRITT as RAFT agent, then the carboxylic group is neutralized.

and methyl acrylate (MA, stabilized, 99%, Sigma-Aldrich) was passed through a column loaded with basic alumina.

4,4′-Azobis(4-cyanovaleric acid) (V-501, 98% Alfa Aesar), 1,3-butanediol diacrylate (DAc, 98%, Sigma-Aldrich), 2-(((dodecylthio)carbonothioyl)thio)propanoate (DoPAT, Lanxess GmbH), *N,N′*-Methylenebisacrylamide (MBA, ≥99.5%, Sigma-Aldrich), sodium carbonate ($NaHCO_3$, ≥99.5, Roth), sodium chloride (NaCl, 99.9%, AnalaR, VWR) were used as received.

Deionized water and 1,4-dioxane (>99.5%, extra-dry, Acros Organic) were employed as solvents.

Deuterium oxide (D_2O, 99.9% isotope purity, Acros Organic) was used as deuterated solvent for the low-field ^{1}H-NMR experiments.

2.2. Synthesis

2.2.1. Synthesis of Poly(methyl acrylate) Networks

Poly(methyl acrylate) networks were synthesized using AIBN as initiator (0.15 equiv.), methyl acrylate (MA, 1000 equiv.) as monomer, 1,3 butanediol diacrylate (DAc, 10 equiv.) as crosslinking agent (DC = 1 mol%, calculated according to Equation (1)), with or without the presence of DoPAT as RAFT agent (1 equiv.), as depicted in Figure S1, Supporting Information.

$$\mathrm{DC} = \frac{\mathrm{mol}_{\mathrm{monomer}}}{\mathrm{mol}_{\mathrm{crosslinking\ agent}}} \times 100 \quad (1)$$

The components were dissolved in 1,4-dioxane (20:80 w/w ratio monomer to solvent). Subsequently, the solution was divided into different vials in order to stop the reaction at different intervals of time. The oxygen was removed by purging each vial with argon for 15 min. The reaction was performed in a heating block preheated at 70 °C and stopped by placing the vial in liquid nitrogen at the desired reaction time. The conversion is calculated gravimetrically according to Equation (2).

$$\mathrm{Conversion}\,[\mathrm{wt\%}] = \frac{m_{\mathrm{final}}}{m_{\mathrm{initial}} \times 0.2} \times 100 \quad (2)$$

where m_{final} is the mass of the crude reaction mixture after evaporation of the solvent and the monomer. The individual masses were obtained with a precision of ±0.1 mg. The mass of the solution after stopping the reaction m_{initial} is multiplied by 0.2 to compensate for the contribution of the solvent to the overall weight.

2.2.2. Synthesis of Poly(sodium acrylate) Networks

For the synthesis of poly(sodium acrylate) networks (PSA), first the poly(acrylic acid) network was synthesized and thereafter the carboxylic group was neutralized with sodium carbonate ($NaHCO_3$) as reported in **Figure 2**.

Poly(acrylic acid) networks were synthesized using 4,4′-Azobis(4-cyanovaleric acid) (V-501, 0.15 equiv.) as initiator, acrylic acid as monomer, and *N,N′*-methylenebisacrylamide (MBA) as crosslinking agent. Furthermore, *S,S*-di((2-methyl)propionic acid) trithiocarbonate (TRITT, 1 equiv.) was used as RAFT agent, while deionized water was used as solvent (20:80 w/w ratio monomer to solvent). For the exact masses the reader is referred to Table S1, Supporting Information. After purging the reaction mixture with argon for 15 min, the polymerization was performed at 70 °C for 16 h. The reaction was stopped by cooling the solution with liquid nitrogen and exposing it to air for quenching the radicals. The extractable fractions were removed by swelling the resultant network for 24 h in an excess of deionized water and removal of the supernatant phase. The procedure was repeated at least three times. Afterward, the network was dried via lyophilization and neutralized.

The neutralization was performed by mixing a known amount of dry polymer with a volume of 0.1 M $NaHCO_3$ (in deionized water) calculated according to Equation (3).

$$V_{\mathrm{NaHCO_3}} = \mathrm{DN}\,\frac{m_{\mathrm{polymer}}}{M_{\mathrm{AA}}\,[\mathrm{NaHCO_3}]} \quad (3)$$

where V is the volume of $NaHCO_3$ ($c = 0.1$ M), DN is the desired degree of neutralization (relative amount of charges, it assumes value between 0 and 1), m is the mass of dry network, and M_{AA} is the molecular weight of acrylic acid. An excess of 10% of $NaHCO_3$ was used to assure full neutralization when targeting DN = 1. After equilibration (16 h), the polymer was washed with deionized water until the pH of the external solution was neutral. As before, the water within the hydrogel was removed via lyophilization.

2.3. Characterization Methods

2.3.1. Determination of the Amount of Extractable Fractions

The influence of the RAFT agent content on the amount of extractable fractions, that is, sol content, was determined as follows: a known volume (1.4 mL) of the crude reaction mixture

Table 1. Summary of the poly(acrylic acid) networks synthesized either via conventional FRP or RAFT polymerization.

Sample	RAFT content [mol%]	Crosslinker [mol%]
FRP-DC0.6	0	0.6
RAFT0.1-DC0.6	0.10	0.6
FRP-DC1	0	1.0
RAFT0.05-DC1	0.05	1.0
RAFT0.1-DC1	0.10	1.0
RAFT0.17-DC1	0.17	1.0
RAFT0.25-DC1	0.25	1.0
RAFT0.5-DC1	0.50	1.0
RAFT1-DC1	1.0	1.0
FRP-DC1.5	0	1.5
RAFT0.1-DC1.5	0.10	1.5
RAFT0.25-DC1.5	0.25	1.5
RAFT0.5-DC2.0	0.5	2.0
FRP-DC3	0	3.0
RAFT0.1-DC3	0.10	3.0
RAFT0.25-DC3	0.25	3.0
FRP-DC5	0	5.0
RAFT0.1-DC5	0.10	5.0
RAFT0.25-DC5	0.25	5.0

The sample abbreviations are denoted, as well as the corresponding RAFT agent and crosslinker contents.

was prepared and subjected to polymerization as described in Section 2.2.2. As the focus is set on the impact of the RAFT agent, the DC was fixed to 1 mol% with respect to the monomer and the amount of RAFT agent was varied from 0 to 1 mol% (refer to **Table 1**). Contrary to the previous procedure, the water used for the removal of the extractable fractions during the three washing cycles was collected and combined. Subsequently, the water was removed in a vacuum oven at 70 °C to afford the sol content as sticky polymer. The amount of extractable fractions was determined upon comparison of the mass of the extractable fractions (m_{sol}) with the mass of polymer initially present in the solution ($m_{tot} = m_{AA} + m_{MBA}$), according Equation (4).

$$\text{Sol content}\,[\%] = \frac{m_{sol}}{m_{tot}} \times 100 \tag{4}$$

2.3.2. Swelling Experiments

In a typical experiment, 10 mg of dry polymer (m_{dry}) was placed on a metal sieve, which was then placed on a metal rack. The metal rack was immersed in a closed Petri dish to prevent evaporation containing NaCl solution (1 wt%). The contact between the dry polymer and the solution occurred exclusively through the sieve. After an equilibration time of 16 h, the sieve and the polymer were gently pressed onto a paper towel for 1 min to remove the excess of water, and weighed ($m_{swollen}$). The degree of swelling (Q) was calculated according to Equation (5).

$$Q = \frac{m_{water}}{m_{dry}} = \frac{m_{swollen} - m_{sieve} - m_{dry}}{m_{dry}} \tag{5}$$

The data reported in the main text are the mean value and the standard deviation of the results obtained in three independent measurements.

2.3.3. Size Exclusion Chromatography

Size-exclusion chromatography (SEC) measurements were conducted on an Agilent 1200 system, consisting of an autosampler, a Plgel 5 µm bead-size guard column (50 × 7.5 mm), one Plgel 5 µm Mixed E column (300 × 7.5 mm), three Plgel 5 µm Mixed C columns (300 × 7.5 mm) a differential refractive index detector and a UV detector. Tetrahydrofuran was employed as eluent at 35 °C with a flow rate of 1 mL min^{-1}. The SEC system was calibrated using linear poly(methyl methacrylate) standards ranging from 800 to 2.2×10^6 g mol^{-1}. In a typical procedure, 100 µL of a 2.0 mg mL^{-1} polymer solution was injected into the system.

2.3.4. Rheology

For the rheological measurements, poly(acrylic acid) hydrogels were prepared in a 7 mL head spaced vial to afford disk-shaped specimens. The vials were filled with 1.4 mL of crude solution, prepared as described in Section 2.2.2. The samples were recorded in the "as-prepared" state, thus without removal of the extractable fractions, as the swelling during the washing, the neutralization, and mostly the drying procedure would lead to cracks in the specimen.

The oscillatory shear rheological measurements were conducted on the strain controlled rheometer ARES-G2 (TA Instruments), using a parallel plate geometry (25 mm). The temperature was set to 20 ± 0.1 °C and controlled via a Peltier element (Advanced Peltier System, TA Instruments). First, an amplitude sweep in the range of $\gamma_0 = 2\ 10^{-3}$ to 10% with an angular frequency of $\omega_1 = 1$ rad s^{-1} was carried out to find the linear viscoelastic regime (LVE). Subsequently, a frequency sweep from $\omega_1 = 0.1$ to 100 rad s^{-1} was conducted using a strain amplitude of $\gamma_0 = 0.1\%$. Finally, the networks were compared using the absolute value of the complex modulus ($|G^*|$) obtained at $\gamma_0 = 0.1\%$ and $\omega_1 = 1$ rad s^{-1} as representative quantity.

2.3.5. ^{1}H-NMR T_2-Relaxation

For the ^{1}H-NMR T_2-relaxation measurements 40–50 mg of dry sample was placed in a sealed 10 mm NMR tube, mixed in a 1 to 9 weight ratio with D_2O, and equilibrated for 2 days. The sample height was adjusted to ensure it is in the region of highest homogeneity of the B_1 magnetic field. The tests were run on a bench-top 20 MHz minispec (Bruker, NF series) and the sample temperature was kept at 30 °C using a BVT3000 unit (Bruker). Before each measurement, the magnetic field was matched and the pulse lengths were determined with the 90° pulse length being below 3 µs. The T_2-relaxation process

covers several orders of magnitude between 10 µs and 4 s. Thus, it is not possible to acquire the full decay in one measurement and the full relaxation curve was obtained employing a combined set of sequences: the magic sandwich echo (MSE) pulse sequence and 4–5 Carr–Purcell–Meiboom–Gill (CMPG) based pulse sequences, which are recorded individually.[53] To compensate the spin locking effect that might occur during the CPMG sequence,[54] XX4[55] and XY16[56] phase cycling sequences were used, as shown in Table S1, Supporting Information. For each measurement, 100 data points were collected and 1024 scans averaged. The MSE was recorded for 50 µs, followed by a XX4 sequence with a pulse separation of $\tau = 50$ µs and the time between two echos of 2 τ. Subsequently, three XY16 pulse sequences were employed with a pulse separation of $\tau =$ 0.04, 0.1, and 1 ms to cover the long tailing of the relaxation curve. In the cases where the decay of the curve is steep at short relaxation times, an additional XX4 sequence with $\tau = 5$ µs was measured to increase the point density in the crucial time frame. A recycle delay of 1 s and no dummy scans were used. From the XY16 cycle every 8th cycle was recorded, while from the XX4 all cycles were traced. The data from all measurements of one sample were collected in a single data file. Subsequently, the solvent signal was subtracted using a single exponential decay fitted to the data above 100 ms, as shown in Figure S4, Supporting Information.[53]

2.3.6. Double Quantum Measurements

The double quantum (DQ) experiments were performed employing the same NMR equipment and sample conditions described earlier. The measurement of DQ coherences is accomplished by the complex Baum–Pines pulse sequence, which was further improved and implemented for the minispec by Saalwächter et al.[57,58] The acquisition parameters, such as pulse length, phase angle, and resonance frequency are optimized for a maximum signal intensity and the imaginary part has to be matched to zero. In these experiments, 70 points of data were recorded for the DQ signal S_{DQ} and the reference intensity S_{ref} with an initial spacing of 0.01 ms and an increment of 1 µs, which was doubled after each eight points. Due to the length of the excitation and reconversion pulse trains, the first point could be measured only after 80 µs, which proved to be insufficient to cover the full build-up curve of the higher crosslinked samples. Therefore, an adapted version of the pulse program was taken with a shortened excitation and reconversion pulse train, both having three pulses.[57] The altered pulse program enabled earlier acquisition of 30 points of data between 10 and 100 µs with an initial spacing of 1 µs, while the spacing was doubled after every eight points of data.

A normalization of S_{DQ} is required to recover the build-up curve undistorted by relaxation effects. Normalization is performed by a stepwise fitting of the long-time tail of the double quantum curve with two single exponential functions. Normalization using Equation (6) yields the so-called build-up curve of the double quantum signal S_{norm}, which consists purely of the network contribution. The detailed process is adapted from Chassé et al. and described in the Supporting Information.[57] Two procedures were applied to extract the inherent distributions of the residual dipolar coupling constants (D_{res}) from the build-up curve. As a first approach, an analytical fit function was applied to the dataset, see Equation (3).[52] The fit takes into account that in inhomogeneous polymer networks, with broad or even multimodal chain length distributions, a single constant D_{res} cannot be applied. As reported by Saalwächter et al., a Gaussian distribution of D_{res} is assumed.[52] Consequently, the mean value of the residual dipolar coupling constant distribution ($D_{res,mean}$) and the width of the distribution (σ) can be derived from the normalized build-up curve DQ data S_{norm}(t) according to Equation (6).[52]

$$S_{norm}(t) = \frac{S_{DQ}}{S_{DQ} + S_{ref} - B\exp(-b\,t) - C\exp(-c\,t)} = 0.5\left(1 - \exp\left(-\frac{0.4\,D_{res,mean}^2 t^2}{1 - 0.8\,\sigma^2 t^2}\right)/\sqrt{1 - 0.8\,\sigma^2 t^2}\right) \quad (6)$$

where S_{DQ} is the double quantum intensity, S_{ref} is the intensity of the reference signal, B, C, b, and c are empirical fit factors, and t is the time. The standard deviation was taken as a measure of the width of the distribution and was renormalized to its average to enable the comparison of different distributions such as the Gaussian and those described later. As a representative example, the normalization procedure is shown in Figure S9, Supporting Information.

As a second method, a Tikhonov regularization was used for an inversion procedure to extract the distribution of the residual dipolar coupling constants, D_{res}, from the normalized DQ data. The procedure was conducted on a program reported by Chassé et al.[48,50] Gaussian kernel functions were used for the regularization, which are reported to fit the DQ build-up curves of hydrogels well.[35] Only raw data up to 2 ms of DQ evolution time was used due to the fast build-up of ≈1 ms and the high noise levels at later data points, which hindered an effective evaluation.

3. Results and Discussion

3.1. Analysis of the Crosslinking Process

In close analogy to the synthesis of linear chains, networks synthesized in the presence of a controlling agent are claimed to have a more homogeneous microstructure due to the assumed gradual growth of polymer chains during the crosslinking process.[32,33] Furthermore, the lower molecular weight of the growing chains at the early stage of the conversion potentially facilitates the diffusion of the chains, favoring intermolecular reactions and limiting the formation of nanogels.[24] Accordingly, a mechanism as reported in Figure 1 was proposed.[33] Herein, the copolymerization of methyl acrylate as monomer and 1,3-butanediol diacrylate as crosslinking agent was studied before the gelation point via SEC to confirm the validity of the aforementioned hypothesis. The reaction scheme is depicted in Figure S2, Supporting Information. Methyl acrylate (MA), which is the ester of the acrylic acid (AA), was chosen as a monomer to suppress enthalpic interaction of the analyte with the stationary phase in the aqueous SEC, which can occur in case of AA samples. The crosslinking agent was used in a

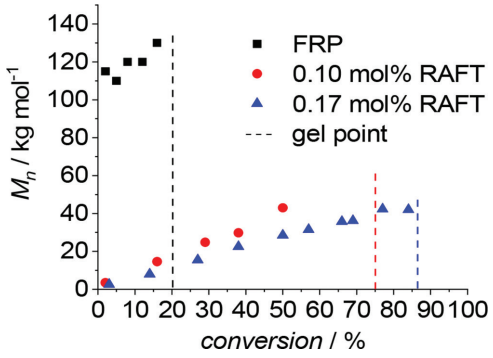

Figure 3. Evolution of the molecular weight (M_n) of the growing chains with conversion using different amounts of RAFT agent: 0 (black square), 0.10 (red square), and 0.17 mol% (blue triangle) and a crosslinker concentration of 1 mol% with respect to the monomer. The M_n was determined by SEC analysis.

concentration of 1 mol% with respect to the monomer (DC = 1 mol%) and, in a first approximation, the copolymerization parameter between the two acrylate monomers is assumed to be equal to 1. For comparison, the reaction was performed with and without the presence of DoPAT as RAFT agent. In the absence of the RAFT agent (FRP), the molecular weight (M_n) of the chain after only 2% conversion is equal to $1.5 \cdot 10^5$ g mol^{-1}, as summarized in **Figure 3**, while the dispersity ($Đ$) is 2.4. A similar SEC trace was obtained after 5% conversion (Figure S2a, gray line, Supporting Information), confirming that the length of the polymer chains is determined only by the ratio of monomer to initiator and not by the conversion. At higher conversion, such as 16%, the molecular weight distribution becomes broader due to the presence of the crosslinking agent, which promotes the crosslinking between different chains to achieve the final network. The gelation occurs at conversion of ≈32%. In contrast, when the mono- and difunctional acrylate derivatives are copolymerized in the presence of 0.10 mol% of DoPAT, after 2% conversion the polymer chains have M_n = 4500 g mol^{-1} and $Đ$ = 1.3 as shown in Figure S2b, black line, Supporting Information.

Moreover, from Figure 3 it is noticeable that the molecular weight of the growing chains gradually increases with the conversion, in agreement with the assumption reported in the literature.[33] The shoulder and broadening of the SEC traces at higher conversion is ascribable to intermolecular reactions between different chains. In this second reported case, the gelation occurs at ≈ 75% conversion. In an additional experiment, the effect of different amount of RAFT agent on the crosslinking process was evaluated. As reported in Figure 3, the higher the amount of DoPAT, the lower the molecular weight of the chain at a fixed conversion. For the SEC traces the reader is directed to Figure S2c, Supporting Information.

It is also shown that the linking between different chains—represented by a shoulder in the SEC traces—occurred at 38% conversion instead of 28% when a higher amount of RAFT agent (0.17 mol%) was present. In addition, the gelation point occurs at a later conversion, equal to 85%. In summary, significant differences were observed during the crosslinking process in the presence of the RAFT agent confirming the validity of the mechanism reported in the literature at early stage of the polymerization (Figure 1).[33] In the next step, the study is extended to understand how the different crosslinking process affects the network topology. Assuming that the observed difference between the FRP and the RAFT mediated crosslinking process are independent from the monomer used, the impact on the network topology was evaluated directly on the targeted poly(acrylic acid) networks.

3.2. Synthesis of Poly(sodium acrylate) Networks

First, the impact of the amount of RAFT agent was evaluated by synthesizing a series of poly(sodium acrylate) (PSA) networks having the same degree of crosslinking (DC = 1 mol%) but different amounts of RAFT agent (TRITT), as summarized in Table 1. The suitability of TRITT in mediating the polymerization of acrylic acid (AA), which is a fundamental prerequisite for the network sythesis as well, is shown in Figure S3, Supporting Information. The network formation was successful for concentrations of RAFT below 0.5 mol%.

In the previous section, as well as in the literature,[59] it is shown that the length of the polymer chains mainly depends on the ratio between RAFT agent and monomer. Therefore, higher amounts of RAFT agent lead to shorter chains, which in turn contain less crosslinking agent. For instance, in the case of 0.50 mol% of RAFT agent, the theoretical number of monomer units per chain is equal to 200 and the number of the crosslinking agent (MBA) is two per chain. As a consequence, a polymer chain would potentially form up to four junction points, under the prerequisite of full conversion and that crosslinker molecules are not incorporated into the same chain twice. Experimentally, it is found instead that the final product is rather a branched polymer than a polymer network as depicted in **Figure 4** on the left. Consequently, the assumption that crosslinks will always interconnect chains has to be discarded and a higher number of crosslinks per chain is found to be necessary to yield a network. To confirm this hypothesis, two networks both containing a theoretical number of four MBA units per chain starting from different amount of TRITT and MBA were synthesized. The idea is conceptually depicted in Figure 4, and the successful network formation in both cases indicates the existence of a critical ratio K between the concentration of DC and RAFT agent. Below this value, the number of potential crosslinking points per chain is not sufficient to guarantee the formation of the network. In the present work K is found to be equal to four crosslinker molecules per chain, thus a maximum of eight junction points.

Accordingly, the amount of extractable fractions increases with increasing the RAFT agent content as shown in **Figure 5**.

In a second step, the amount of RAFT agent was fixed to 0, 0.10, and 0.25 mol% with respect to the monomer and the amount of crosslinking agent was systematically increased from 0.6 to 5.0 mol% with respect to the monomer, as summarized in Table 1. This set of data serves for understanding how the presence of the RAFT agent affects the mechanical and swelling ability of the network at different DC.

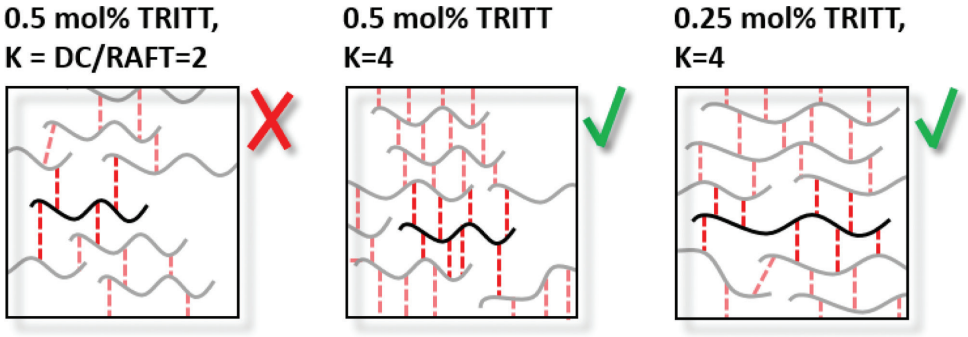

Figure 4. Theoretical description of the influence of the ratio RAFT agent (TRITT) content to degree of crosslinking. Highlighted is the impact of the number of crosslinking points per chain.

3.3. Swelling Experiments

Swelling experiments were conducted to obtain a first insight into the average crosslink density. The results, listed in Table 1, show an increase in the degree of swelling (Q), calculated according to Equation (5), from $Q = 29.1 \pm 1.8$ to $Q = 39.2 \pm 0.8$ with increasing the amount of TRITT used during the synthesis from 0 to 0.25 mol%. The data indicate a less densely crosslinked microstructure in case of RAFT polymerized samples.

Concerning the series of PSAs having different degree of crosslinking, it was observed that the higher the DC, the lower is the Q, regardless of the synthetic approach employed. The relationship between DC and Q is described by the Flory–Rehner theory as shown in Equation (7).[4]

$$Q = A \times DC^{B} \tag{7}$$

where A and B are two empirical factors. The theory was developed for non-charged networks and predicts a value of $B = -0.60$ for ideal networks.[4]

In **Figure 6** it is shown that for the polyelectrolyte hydrogels synthesized via FRP $B = -0.55$, while for the RAFT mediated networks $B = -0.54$ and -0.64 when using 0.10 and 0.25 mol% of TRITT, respectively. All the scaling exponents are similar to the predicted $B = -0.60$ value, indicating that the prediction of the Flory–Rehner theory can be applied as the presence of the charges affects the prefactor A but not B. However, further investigation is necessary to better elucidate the network topology.

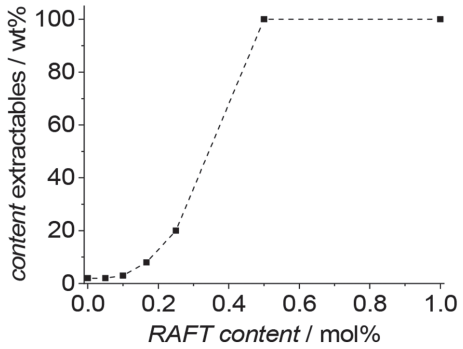

Figure 5. Amount of extractable fractions obtained after the synthesis of the PAA networks in the presence of different amount of RAFT agent. The line is meant as a guide for the eye.

3.4. Rheology

The rheological measurements were conducted on poly(acrylic acid) networks in the "as-prepared" state and the complex modulus $|G^*|$ was probed. The complex modulus $|G^*|$ consists of the storage modulus G', which describes the elasticity of the sample, and the loss modulus G'', which describes its viscous part. The phantom model can be employed to describe the elastic deformation of a polymer network. The model assumes freely moving chains and that the time-averaged, mean positions of the crosslinks are affine to the macroscopic deformation, that is, all parts of the network are displaced in the same direction and by the same extent, while there are dynamic thermal fluctuations around these mean positions. Accordingly, the average length of a mesh in hydrogel network M_c can be estimated from the storage modulus G' using Equation (8).[8]

$$G' = \left(1 - \frac{2}{f}\right) \frac{RT\rho\nu^{1/3}\nu_0^{2/3}}{M_c} \tag{8}$$

where f is the functionality of the crosslinks (4 for tetrafunctional linker), R is the gas constant, T is the absolute temperature, ρ is the monomer density, ν the polymer volume fraction, and ν_0 is the polymer volume fraction during gel formation, with $\nu_0 = \nu = 0.2$ g g^{-1} in the "as-prepared" state.[60] The phantom model is appropriate for dilute networks obtained by statistical crosslinking.[61]

The rheological measurements show that the $|G^*|$ moduli decrease from 15 to 2.5 kPa for samples polymerized with 0 and 0.25 mol% RAFT agent and constant 1 mol% of crosslinking agent, as depicted in **Figure 7**a. Moreover, the $|G^*|$ moduli increase with increasing amount of crosslinker independently of the synthetic approach as shown in Figure 7b. A decrease in the complex modulus is associated with a lower apparent crosslink density, in agreement with what is observed during the swelling experiments. The differences in the moduli between FRP and RAFT polymerized samples become less pronounced when diminishing the amount of RAFT agent or with increasing amount of crosslinker, and no differences are observed when

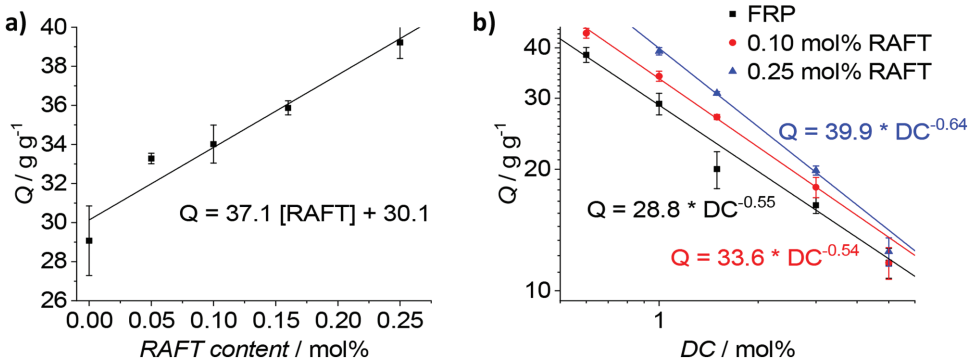

Figure 6. The degree of swelling (Q) in 1 wt% NaCl aqueous solution obtained for a series of PSA networks having a) DC = 1 mol% and different amounts of RAFT agent, and b) 0 (black symbols), 0.10 (red symbols), and 0.25 mol% (blue symbols) of TRITT and different DC.

the DC ≥ 3 mol%, as shown in Figure 7b. This hypothesis is also confirmed by the calculations of M_c, obtained using Equation (8), which revealed that the apparent chain length between two junction points is larger than the theoretical value in each case, but it is more significant for the RAFT mediated samples.

The disagreement between the theoretical and experimental M_c values are shown in Figure 7c and can be ascribed to the presence of nonelastic defects such as primary loops and unreacted moieties. By comparing the calculated and the theoretical value of the molecular weight of the elastic chain, the crosslinking efficiency k can be obtained according to Equation (9).[61] In a first approximation, the lower the value of k, the higher is the amount of defects in a network.

$$k = 100\frac{M_{\text{target}}}{M_c} = 100\frac{M_{\text{AA}}}{2DC\,M_c} \tag{9}$$

where M_{AA} is the molecular weight of the monomer acrylic acid and DC is the degree of crosslinking. The calculated crosslinking efficiencies are depicted in Figure 7d and were found in the range between 3% and 27%. It was shown that with increasing the RAFT content k decreases. Furthermore, the differences between RAFT polymerized and FRP samples vanish for high degrees of crosslinking.

In addition, the dissipation factor tan δ, which is the well-known ratio between the loss modulus G'' and the storage modulus G', was calculated according to Equation (10).

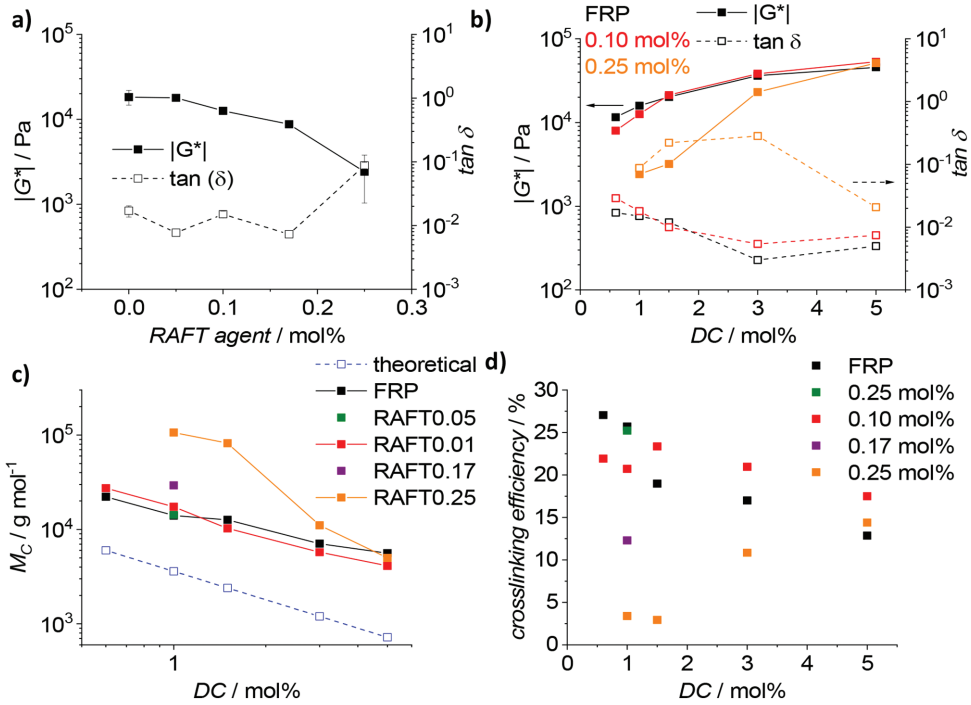

Figure 7. The absolute value of the complex modulus |G*| (full symbol) and tan δ (empty symbols) is reported for a series of PSA networks having a) DC = 1 mol% and different amounts of RAFT agent, and b) different DC but fixed amounts of RAFT agents, such as 0 (black symbols), 0.10 (red symbols), and 0.25 mol% (orange symbols). c) Theoretical (blue empty symbol) and experimental (full symbol) molecular weight of the elastic chain (M_c). The experimental value was calculated using the phantom according to Equation (8). d) Crosslinking efficiency estimated from the comparison of the theoretical and experimental M_c value, according to Equation (9).

$$\tan\delta = \frac{G''}{G'} \tag{10}$$

Van Den Bulcke et al. observed that in case of hydrogels $|G^*| \approx G'$, and thus low values for tan δ are to be expected.[62] The samples containing amounts of RAFT agent up to 0.17 mol% and $DC = 1$ mol% provide similar values of tan $\delta \approx 0.01$ as the FRP sample, as shown in Figure 7a. Interestingly, tan δ increases to ≈0.1 for the samples with 0.25 mol% of RAFT agent. The higher values of tan δ could be caused by the higher content of soluble fragments of 20 wt%, which were found by the extraction experiments. The mobile chains are characterized by a higher degree of freedom, and thus leads to a higher dissipation of energy.

3.5. Transverse Relaxation

The dominant relaxation mode in the transverse ^{1}H-NMR relaxation arises from the orientation-dependent homonuclear dipolar couplings D of neighboring proton spins along the chain. The orientation dependency is characterized by the distance r between the spins and the angle Θ to the applied magnetic field B_0 according to Equation (11).[63]

$$D = \frac{\kappa}{2r^3}(3\cos^2\Theta - 1) \tag{11}$$

with the proportionality factor $\kappa = 240$ kHz Å^3 for ^{1}H–^{1}H spin pairs.[63] Therefore, the relaxation behavior can be linked to the orientation autocorrelation function of chain segments as the most relevant description of molecular dynamics.[58,64] The crosslinking points in networks bring additional constraints into the system and result in a long-time plateau of the autocorrelation function. The amount of residual correlation, which is related to the crosslinking density, can be measured either by a direct analysis of the residual dipolar couplings D_{res}, as described later in the double quantum section, or by analyzing transverse relaxation decays. The transverse relaxation of the magnetization, also called T_2-relaxation, is related to the autocorrelation function of the motion and thus it is mostly affected by slow motions. Consequently, the molecular dynamics of polymer chain segments in a network, as probed by T_2-NMR, can be linked to the network structure via its hindered dynamics.

Apart from the junction points, the amount of charges present at the polymer backbone might influence the relaxation behavior due to its effect on the magnetic susceptibility of the sample and on the motion of the chains.[65] Therefore, a T_2-relaxation study of samples with varying charge fractions from 0 to 100 mol% with respect to the acrylic acid was conducted. It was found that the influence of the charges on the measured network mobility can be neglected when the charge content is higher than 50 mol%. For more details, the reader is referred to Figure S5, Supporting Information.

The T_2-relaxation curves of the fully charged samples are depicted in **Figure 8** and Figure S6a, Supporting Information, revealing that with decreasing RAFT content and increasing the DC a faster relaxation decay is observed. The fast relaxation reflects a more rigid network structure and confirms the rheological finding of lower apparent crosslinking densities of RAFT samples. As before, the difference arising from the adopted synthetic procedure diminish at higher DC.

To further process the data, first an empirical stretched exponential curve is fitted to the data according to Equation (12).

$$I(t) = A\exp\left(-\frac{t}{\tau_1}\right)^{\beta} \tag{12}$$

where time is t, the normalization pre-factor A, the empirical time constant τ_1 and the stretch factor β. According to Böhmer et al. the empirical stretch factor β is inversely proportional to the width of the relaxation rate distribution in decades.[66,67] Thus, β can be taken as a measure for the inhomogeneity in mobility of the network and was found to be in the range of 0.42–0.62, independently from the polymerization procedure, as shown in Figure S7b, Supporting Information. In case of a more homogeneous network, a narrower distribution of the relaxation time is to be expected. According to our measurements, most of the RAFT mediated networks have lower stretching factors than the FRP ones, which is most likely correlated to a higher heterogeneity of the FRP network topology. The factor τ_1 refers to the characteristic

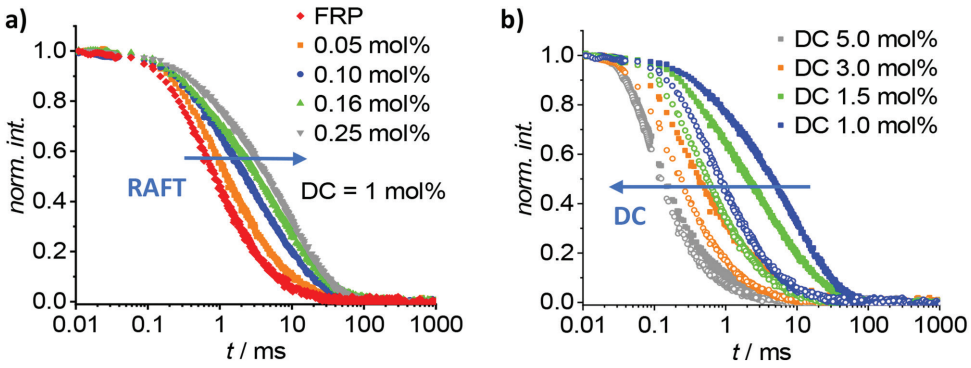

Figure 8. a) T_2-relaxation curves of poly(sodium acrylate) hydrogels with DC = 1.0 mol% and different amount of RAFT agent shown in the legend. b) T_2-relaxation curves of hydrogels with DC ranging from 0.6 to 5 mol% synthesized via FRP, empty symbols, or with 0.25 mol% RAFT agent, full symbols.

relaxation time and provides an insight into the average mobility of the networks. It was found that the parameter τ_1 is linearly dependent on the RAFT agent content, as shown in Figure S7c, Supporting Information. Thus, the networks are more mobile at higher RAFT content, confirming the previous findings from the rheological measurements and the swelling experiments of an apparent lower DC. In addition, the parameter τ_1 revealed a power law dependency on the degree of crosslinking, which reflects the loss of mobility due to the additional crosslinks, as depicted in Figure S7d, Supporting Information.

A second way for data treatment involves the use of an inverse Laplace transformation (ILT) for the deconvolution of the T_2-relaxation data. The ILT was performed using the Contin approach, and provides information about the relaxation rates present in the networks based on exponential fit functions. The T_2-relaxation rate distributions are displayed in **Figure 9**a,b and Figure S6b, Supporting Information and show a shift of the peak maxima and the average values to higher rates with decreasing RAFT agent content and increasing of the DC, congruently with the previous data.

In this second approach, the inhomogeneity of the mobility was determined by calculating the standard deviation σ_{log} as description of the width of the T_2-relaxation rate distributions. In order to ensure that all points have an equal spacing and thus an equal weight in the calculation of the standard deviation, the *x*-axis was linearized by taking the logarithm giving the linearized standard deviation σ_{lin}. This approach enables the comparison of distributions, which are different in shape and well separated on the logarithmic scale. Subsequently, the standard deviation σ_{log} was obtained by back transformation of σ_{lin} by Equation (13).

$$\sigma_{log} = 10^{\sigma_{lin}} \tag{13}$$

The findings are in agreement with those obtained using Equation (12), where the width distribution increases with increasing the RAFT content (Figure 9c). In addition, the mobility distribution of the RAFT samples becomes narrower toward extreme DC in both directions, while for FRP samples the trend is less pronounced (Figure 9d). Since it is assumed that a broader distribution is associated with a less homogeneous network microstructure, the next step is to understand whether the heterogeneity arises from a more heterogeneous mesh size distribution or from a higher content of mobile network defects, such as dangling ends. For this purpose, DQ measurements were performed, as reported in the following section.

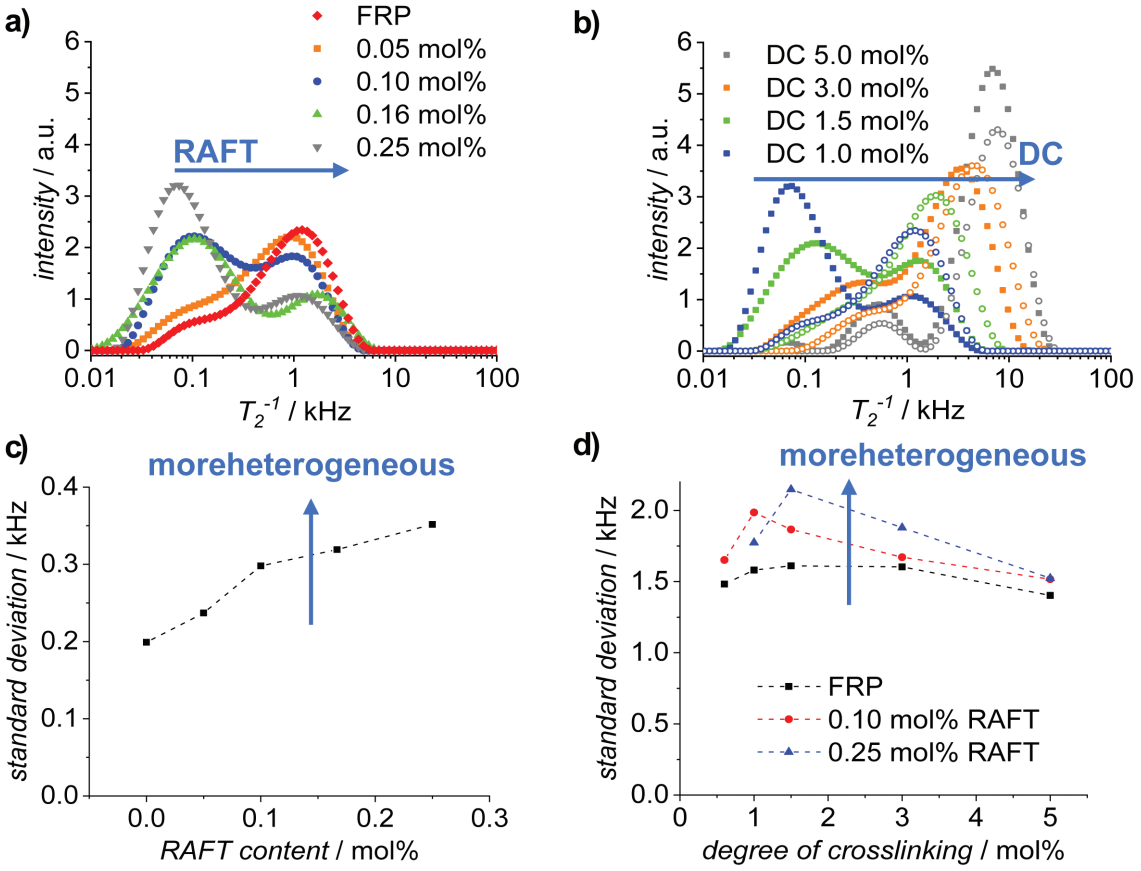

Figure 9. T_2-relaxation rate distributions as obtained by the inverse Laplace transformation. Dependency on the a) RAFT agent content during synthesis at DC = 1 mol% and b) the degree of crosslinking, with a RAFT agent content of 0 (full symbols) and 0.1 mol% (empty symbols). Standard deviation of the distributions of the latter at c) different RAFT agent contents (DC = 1 mol%) and d) different DC, with the RAFT agent contents displayed in the legend.

3.6. Double Quantum Measurements

Double quantum measurements provide a direct access to the residual dipolar coupling D_{res} and thus the molecular dynamics.[58] In the previous section, it was shown that the RAFT samples exhibit broader T_2-relaxation rate distributions. However, the source of the underlying heterogeneity could not be assigned since both, network defects and the mesh size distribution could contribute. To answer the remaining question, DQ measurements were performed. The pulse sequence yields the reference signal S_{ref} and the double quantum signal S_{DQ}, as shown in Figure S8, Supporting Information. To evaluate the content of mobile species in the networks, the DQ data could be described by a tri-exponential function according to Equation (14).[52]

$$\frac{S_{ref}(t) - S_{DQ}(t)}{S_{ref}(t=0)} = A_n \exp(-a\,t) + B_n \exp(-b\,t) + C_n \exp(-c\,t) \quad (14)$$

where $A_n + B_n + C_n = 1$ and t is the time. The pre-exponential factor A_n represents the contribution of the elastic network to the overall signal, B_n the amount of mobile network fractions, for example, network defects like loops, or dangling ends, and C_n the content of mobile components, such as solvent, or extractables. The empirical factors a, b, and c serve as the characteristic relaxation rates of the fractions A_n, B_n, and C_n. The network and the network defects relax faster than the mobile components due to the higher rigidity, introduced by the crosslinking points ($a > b > c$).

The relative content of mobile network defects in fraction C_n could not be separated from the solvent and the potentially remaining extractables. Thus, only the content of B_n was considered as a measure for the amount of defects. It was observed that when the RAFT content is increased, the content of the mobile fraction B_n increases, indicating a higher amount of defects, such as dangling ends and loops as depicted in **Figure 10**a. The amount of mobile fractions B_n increases with decreasing DC, as shown in Figure 10b, which can be explained by a lower content of dangling chains due to the high crosslink density.

Subsequently, the structure of the effective elastic network was evaluated without defects, by renormalizing the double quantum signal S_{DQ} according to the procedure described in the Experimental Section. The samples with increasing crosslink density revealed that the build-up of the double quantum coherence is faster, which is an indication for the increased rigidity of the polymer structures, as depicted in **Figure 11**b and Figure S9, Supporting Information. Additionally, the build-up curves of PSA network with DC = 1 mol% with different amount of RAFT agent were measured. The results showed a slower DQ build-up, and thus more flexible network microstructures, compared to the FRP. This might suggest that the RAFT samples have larger mesh sizes than their FRP counterparts, or likely that the FRP samples have more entanglements, which act as additional crosslinks. The differences in mobility among the RAFT based samples at DC = 1 mol% could not be resolved, since the curves overlapped, as shown in Figure 11a, which could indicate equally large mesh sizes.

A Tikhonov-regularization and an analytical fit function assuming a Gaussian distribution of D_{res} were applied to extract the inherent distributions of the residual dipolar coupling constants as described in the Experimental Section. The D_{res} distributions obtained by the Tikhonov-regularization are depicted in Figure S11, Supporting Information. It was found for both applied methods, the Gaussian approach and the Tikhonov regularization, that the standard deviations of the distributions remain independent of the crosslink density and the RAFT agent content, as shown in Figure 11c,d.

The standard deviations of the 3 and 5 mol% crosslinked sample synthesized using 0.25 mol% of TRITT, obtained by the Gaussian approach, were not considered as the measured $D_{res,mean} \approx 0$ lead to a singularity. The results suggest that the mesh size distributions are equally heterogeneous for both FRP and RAFT polymerization. Thus, the heterogeneity in mobility arises from nonelastic defects, such as dangling ends and loops. Based on our findings, especially those described in the current section, a new picture of the RAFT based network formation mechanism is proposed. In detail, it was generally observed that higher RAFT agent content leads to shorter chain with, on average, fewer crosslinking units per chain. Thus, the formed junction points are distributed over more chains leading to a higher number of dangling ends. The extreme case is one crosslinking point per chain, as shown in **Figure 12**a,

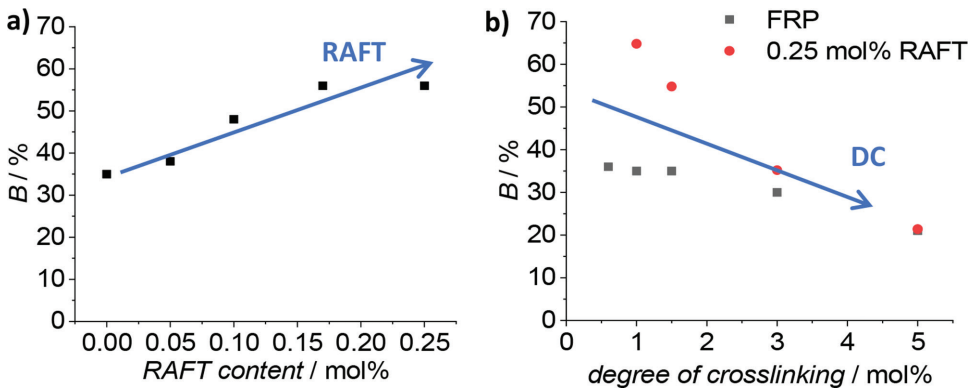

Figure 10. Relative amount of the moderately mobile fraction B, that is, loops and dangling chains, as obtained according to Equation (12) measured for a) different amounts of RAFT agent at DC = 1 mol%, and b) different DC at RAFT agent contents of 0 (black) and 0.25 mol% (red).

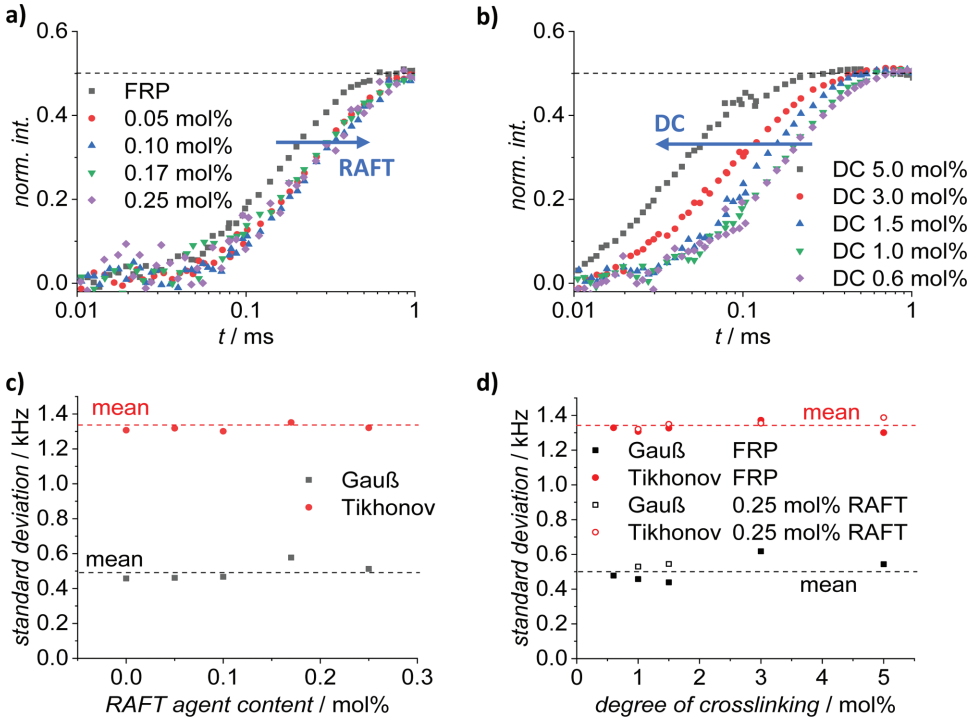

Figure 11. ^{1}H-double quantum (DQ) build-up curves of PSA hydrogels measured with a) different amount of RAFT agent and b) different degree of crosslinking. The inherent D_{res} distributions are shown in Figure S11, Supporting Information. The calculated standard deviation of the D_{res} distributions of the build-up curves at varying DC reveal c) the dependency on the RAFT agent content and d) on the DC with a RAFT agent content of 0 (full symbols), and 0.10 mol% (empty symbols) of TRITT.

where no network formation was observed. When reducing the RAFT agent content, the crosslink density per chain increases (Figure 12b). Here, the network formation is achieved, but the network still contains many mobile parts, for example, dangling ends. Eventually, at a minimal amount of RAFT agent the length of the elastic chain is comparable to the one obtained in the FRP and the contribution of the mobile content is negligible, indicating fewer network defects, as reported in Figure 12c.

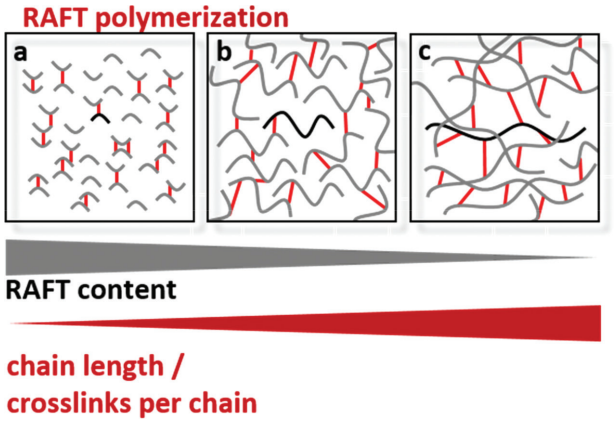

Figure 12. Representation of the new proposed theoretical description of PSA network synthesized via RAFT mediated polymerization. a) High RAFT content leads to a not sufficient number of crosslinking point per chain for the achievement of network formation. b) Decreasing the amount of RAFT agent yield networks with high content of dangling ends and c) at low amounts of RAFT agent the chains are bound multiple times to the network, limiting the amount of dangling ends, that is, network defects.

4. Conclusion

The impact of two different synthetic procedures, that is, RAFT polymerization and conventional FRP, on the topology of the resulting networks was compared for poly(sodium acrylate) based hydrogels.

The crosslinking process performed with and without the presence of the RAFT agent showed a significant influence of the controlling agent on the network formation. The presence of the RAFT agent led to a narrower molecular weight distribution, and to a constant growth of the chains during conversion. Moreover, the usage of a controlling agent lowered the length of the polymer chains and thus by statistics the average number of crosslinking molecules per chain, which drastically affected the network formation. In case of PSA networks, a critical ratio of DC to RAFT agent equal to 4 was found, yielding a theoretical amount of four MBA units per chain, which could form crosslinks. With lower number of crosslinker molecules per chain hydrogels cannot be obtained.

Increasing the amount of RAFT agent also led to higher degree of swelling from $Q = 29.1 \pm 1.8$ up to $Q = 39.2 \pm 0.8$ when 0.25 mol% of TRITT were used with respect to the monomer, which can be beneficial for applications where

a high water absorbency is required. This high swelling degree is associated with a decrease in the elastic modulus of the network. Assumptions on the network inhomogeneity were concluded from the mobility distribution, as obtained by low-field ^{1}H-NMR techniques such as T_2-relaxation and DQ measurements. In detail, the T_2-relaxation measurements showed a broader mobility distribution in case of the RAFT mediated crosslinking process. Independently from the broadness of the distribution, the networks synthesized with a higher RAFT agent content showed a higher mobility. This result, together with the general trend observed in the previous analysis, indicates that increasing the amount of RAFT agent leads to less densely crosslinked networks. Lastly, the DQ measurements revealed that the increase in mobility and in the swelling ability, as well as the decrease in the mechanical properties can be attributed to a higher amount of defects, such as dangling ends, rather than to a less homogeneous mesh size distribution. Upon subtraction of the defects indeed, the mobility distribution was comparable independently from the employed synthetic approach. The higher amount of dangling ends is due to the shorter length of the polymer chains, and thus needs to be taken into account in following studies for the investigation of, for instance, the mesh size distribution. In case of further studies however, the RAFT agent concentration should be chosen low enough that the chain lengths are similar for the compared techniques. Equal chain lengths is an important prerequisite to ensure that the findings are solely associated on the influence of the RAFT agent on the crosslinking process.

Supporting Information

Supporting Information is available from the Wiley Online Library or from the author.

Acknowledgements

F.C. and C.P. contributed equally to this work. The authors acknowledge financial support from the "Sonderforschungsbereich 1176" (project C1) funded by the German Research Council (DFG) as well as the Karlsruhe Institute of Technology (KIT). L.A. acknowledges funding from the DFG through the grant number WI 1911/24-1.

Open access funding enabled and organized by Projekt DEAL.

Conflict of Interest

The authors declare no conflict of interest.

Keywords

hydrogels, networks, NMR relaxometry, reversible addition–fragmentation chain transfer polymerization, rheology

Received: September 12, 2019
Revised: November 13, 2019
Published online: December 9, 2019

[1] J. E. Mark, *Physical Properties of Polymers Handbook*, 2nd ed., Springer, New York **2007**.
[2] J. C. Hernández-Ortiz, E. Vivaldo-Lima, *Handbook of Polymer Synthesis, Characterization, and Processing*, John Wiley & Sons, Hoboken, NJ. **2013**.
[3] P. J. Flory, J. Rehner, *J. Chem. Phys.* **1943**, *11*, 512.
[4] P. J. Flory, *Principles of Polymer Chemistry*, Cornell University Press, Ithaca, NY **1953**.
[5] F. Ganji, F. S. Vasheghani, F. E. Vasheghani, *Iran Polym. J.* **2010**, *19*, 375.
[6] S. J. Buwalda, K. W. M. Boere, P. J. Dijkstra, J. Feijen, T. Vermonden, W. E. Hennink, *J. Controlled Release* **2014**, *190*, 254.
[7] H. H. Hooper, J. P. Baker, H. W. Blanch, J. M. Prausnitz, *Macromolecules* **1990**, *23*, 1096.
[8] W. Oppermann, in *Polyelectrolyte Gels*, American Chemical Society, Washington, DC **1992**, p. 159.
[9] F. L. Buchholz, *J. Chem. Educ.* **1996**, *73*, 512.
[10] K. Ohmura, Rodman Media Corp (US), Nonwoven Industries, https://www.nonwovens-industry.com/issues/2015-11-01/view_far-east-report/an-update-on-the-global-superabsorbent-polymer-producers/ (accessed: September 2019).
[11] K. Pulidindi, S. Chakraborty, *Global Market Insight Polymer and Advanced Materials*, https://www.gminsights.com/industry-analysis/superabsorbent-polymers-sap-market" (accessed: September 2019).
[12] F. Masuda, in *Superabsorbent Polymers*, American Chemical Society, Washington, DC **1994**, p. 88.
[13] K. Kazanskii, S. Dubrovskii, in *Polyelectrolytes Hydrogels Chromatographic Materials*, Springer, Berlin **1992**, p. 97.
[14] M. J. Zohuriaan-Mehr, H. Omidian, S. Doroudiani, K. Kabiri, *J. Mater. Sci.* **2010**, *45*, 5711.
[15] J. Höpfner, C. Klein, M. Wilhelm, *Macromol. Rapid Commun.* **2010**, *31*, 1337.
[16] J. Höpfner, T. Richter, P. Košovan, C. Holm, M. Wilhelm, in *Intelligent Hydrogels*, Springer, Berlin **2013**, p. 247.
[17] L. Arens, J. B. Albrecht, J. Höpfner, K. Schlag, A. Habicht, S. Seiffert, M. Wilhelm, *Macromol. Chem. Phys.* **2017**, *218*, 1700237.
[18] L. Arens, F. Weißenfeld, C. O. Klein, K. Schlag, M. Wilhelm, *Adv. Sci.* **2017**, *4*, 1700112.
[19] M. A. Haque, T. Kurokawa, J. P. Gong, *Polymer* **2012**, *53*, 1805.
[20] Y. Gu, J. Zhao, J. A. Johnson, *Trends Chem.* **2019**, *1*, 318.
[21] J. Wang, T. S. Lin, Y. Gu, R. Wang, B. D. Olsen, J. A. Johnson, *ACS Macro Lett.* **2018**, *7*, 244.
[22] M. Zhong, R. Wang, K. Kawamoto, B. D. Olsen, J. A. Johnson, *Science* **2016**, *353*, 1264.
[23] E. Mendes, P. Lindner, M. Buzier, F. Boué, J. Bastide, *Phys. Rev. Lett.* **1991**, *66*, 1595.
[24] S. Seiffert, *Polym. Chem.* **2017**, *8*, 4472.
[25] Y. Gu, K. Kawamoto, M. Zhong, M. Chen, M. J. A. Hore, A. M. Jordan, L. T. J. Korley, B. D. Olsen, J. A. Johnson, *Proc. Natl. Acad. Sci. U. S. A.* **2017**, *114*, 4875.
[26] T. Sakai, U.-I. Chung, T. Matsunaga, M. Shibayama, Y. Yamamoto, C. Ito, R. Yoshida, S. Suzuki, N. Sasaki, *Macromolecules* **2008**, *41*, 5379.
[27] G. Hild, *Prog. Polym. Sci.* **1998**, *23*, 1019.
[28] H. Zhou, J. Woo, A. M. Cok, M. Wang, B. D. Olsen, J. A. Johnson, *Proc. Natl. Acad. Sci. U. S. A.* **2012**, *109*, 19119.
[29] F. Lange, K. Schwenke, M. Kurakazu, Y. Akagi, U. I. Chung, M. Lang, J. U. Sommer, T. Sakai, K. Saalwächter, *Macromolecules* **2011**, *44*, 9666.
[30] P. Nesvadba, *Encyclopedia of Radicals in Chemistry, Biology and Materials*, John Wiley & Sons, Hoboken, NJ **2012**.
[31] N. Ide, T. Fukuda, *Macromolecules* **1999**, *32*, 95.
[32] N. Ide, T. Fukuda, *Macromolecules* **1997**, *30*, 4268.
[33] R. Henkel, P. Vana, *Macromol. Chem. Phys.* **2014**, *215*, 182.
[34] Q. Yu, Y. Zhu, Y. Ding, S. Zhu, *Macromol. Chem. Phys.* **2008**, *209*, 551.

[35] T. Norisuye, T. Morinaga, Q. Tran-Cong-Miyata, A. Goto, T. Fukuda, M. Shibayama, *Polymer* **2005**, *46*, 1982.
[36] A. R. Kannurpatti, K. J. Anderson, J. W. Anseth, C. N. Bowman, *J. Polym. Sci., Part B: Polym. Phys.* **1997**, *35*, 2297.
[37] A. J. Scott, A. Nabifar, A. Penlidis, *Macromol. React. Eng.* **2014**, *8*, 639.
[38] L. Arens, M. Wilhelm, *Macromol. Chem. Phys.* **2019**, *220*, 1900093.
[39] F. D. Lorenzo, S. Seiffert, *Polym. Chem.* **2015**, *6*, 5515.
[40] K. Urayama, T. Kawamura, S. Kohjiya, *Polymer* **2009**, *50*, 347.
[41] S. Seiffert, *Prog. Polym. Sci.* **2017**, *66*, 1.
[42] D. C. Tuncaboylu, M. Sahin, A. Argun, W. Oppermann, O. Okay, *Macromolecules* **2012**, *45*, 1991.
[43] K. Nishi, H. Asai, K. Fujii, Y. S. Han, T. H. Kim, T. Sakai, M. Shibayama, *Macromolecules* **2014**, *47*, 1801.
[44] F. Cavalli, H. Mutlu, S. O. Steinmueller, L. Barner, *Polym. Chem.* **2017**, *8*, 3778.
[45] D. Estupiñán, C. Barner-Kowollik, L. Barner, *Angew. Chem., Int. Ed.* **2018**, *57*, 5925.
[46] S. Piluso, R. Vukićević, U. Nöchel, S. Braune, A. Lendlein, A. T. Neffe, *Eur. Polym. J.* **2018**, *100*, 77.
[47] J. Wang, T.-S. Lin, Y. Gu, R. Wang, B. D. Olsen, J. A. Johnson, *ACS Macro Lett.* **2018**, *7*, 244.
[48] K. Saalwächter, S. Seiffert, *Soft Matter* **2018**, *14*, 1976.
[49] P. DePhillips, A. M. Lenhoff, *J. Chromatogr. A* **2000**, *883*, 39.
[50] M. Hess, E. Roeben, A. Habicht, S. Seiffert, A. M. Schmidt, *Soft Matter* **2019**, *15*, 842.
[51] K. Saalwächter, J.-U. Sommer, *Macromol. Rapid Commun.* **2007**, *28*, 1455.
[52] K. Saalwächter, in *Modern Magnetic Resonance* (Ed: G. Webb), Springer, Cham, Switzerland **2018**, p. 755.
[53] J. Höpfner, G. Guthausen, K. Saalwächter, M. Wilhelm, *Macromolecules* **2014**, *47*, 4251.
[54] B. J. Suh, F. Borsa, D. R. Torgeson, *J. Magn. Reson., Ser. A* **1994**, *110*, 58.
[55] A. J. Shaka, S. P. Rucker, A. Pines, *J. Magn. Reson* **1988**, *77*, 606.
[56] T. Gullion, S. Louis, D. B. Baker, *J. Magn. Reson* **1990**, *89*, 479.
[57] W. Chassé, J. L. Valentín, G. D. Genesky, C. Cohen, K. Saalwächter, *J. Chem. Phys.* **2011**, *134*, 044907.
[58] K. Saalwächter, *Prog. Nucl. Magn. Reson. Spectrosc.* **2007**, *51*, 1.
[59] S. Perrier, *Macromolecules* **2017**, *50*, 7433.
[60] H. Wack, *Ph.D. Thesis*, Fraunhofer Institute for Environmental, Safety, and Energy Technology, Oberhausen, Germany **2006**.
[61] R. Hernández, D. López, C. Mijangos, *J. Appl. Polym. Sci.* **2006**, *102*, 5789.
[62] A. I. Van Den Bulcke, B. Bogdanov, N. De Rooze, E. H. Schacht, M. Cornelissen, H. Berghmans, *Biomacromolecules* **2000**, *1*, 31.
[63] F. Kramer, M. V. Deshmukh, H. Kessler, S. J. Glaser, *Concepts Magn. Reson.* **2004**, *21A*, 10.
[64] N. Bloembergen, E. M. Purcell, R. V. Pound, *Phys. Rev.* **1948**, *73*, 679.
[65] B. Bleaney, *J. Magn. Reson* **1972**, *8*, 91.
[66] R. Böhmer, K. L. Ngai, C. A. Angell, D. J. Plazek, *J. Chem. Phys.* **1993**, *99*, 4201.
[67] P. K. Dixon, *Phys. Rev. B* **1990**, *42*, 8179.